PCCP

PAPER

View Article Online
View Journal | View Issue

Cite this: *Phys. Chem. Chem. Phys.*, 2018, **20**, 21693

Li doped kagome spin liquid compounds†

Wei Jiang, [a] Huaqing Huang, [a] Jia-Wei Mei*[b] and Feng Liu*[a]

Received 20th May 2018,
Accepted 31st July 2018

DOI: 10.1039/c8cp03219j

rsc.li/pccp

Herbertsmithite and Zn-doped barlowite are two compounds for experimental realization of two-dimensional kagome spin liquids. Theoretically, it has been proposed that charge doping a quantum spin liquid gives rise to exotic metallic states, such as high-temperature superconductivity. However, one recent experiment on herbertsmithite with successful Li-doping surprisingly showed an insulating state even under a heavily doped scenario, which cannot be explained by previous theories. Using first-principles calculations, we performed a comprehensive study on the Li intercalation doping effect of these two compounds. For the Li-doped herbertsmithite, we identified the optimized Li position at the Cl–$(OH)_3$–Cl pentahedron site instead of the previously speculated Cl–$(OH)_3$ tetrahedral site. With increasing Li doping concentration, saturation magnetization decreases linearly due to charge transfer from Li to Cu ions. Moreover, we found that Li forms chemical bonds with nearby $(OH)^-$ and Cl^- ions, which lowers the surrounding chemical potential and traps electrons, as evidenced by the localized charge distribution, explaining the insulating behavior measured experimentally. Though a different structure from herbertsmithite, Zn-doped barlowite shows the same features upon Li doping. We conclude that Li doping this family of kagome spin liquids cannot realize exotic metallic states, and other methods should be further explored, such as element substitution with those having different valence electrons.

1 Introduction

When subjected to strong geometric frustrations, quantum spin systems may achieve paramagnetic ground states dubbed resonance valance bond (RVB) or quantum spin liquid (QSL) states.[1] QSLs are unambiguous Mott insulators whose charge gap is not associated with any symmetry breaking[1] and are characterized by a pattern of long-range quantum entanglements that have no classical counterparts.[2–4] Upon charge doping in QSLs, exotic quantum states may evolve, such as the high-temperature superconductivity predicted in Anderson's doped RVB theory,[1] a metallic pseudogap state that has small hole-like Fermi pockets[5–8] dubbed a fractional Fermi liquid,[6,9,10] and Luttinger-volume violating Fermi liquids.[7]

Kagome Heisenberg antiferromagnets are promising systems for the pursuit of QSLs.[11–21] Herbertsmithite $[ZnCu_3(OH)_6Cl_2]$[22–26] and Zn-doped barlowite $[ZnCu_3(OH)_6FBr]$[27] are two reported compounds for two-dimensional (2D) realization of kagome spin liquids with a gapped ground state. In herbertsmithite, inelastic neutron scattering measurements have detected a continuum of spin excitations[25] while nuclear magnetic resonance (NMR) measurements suggest a finite gap at low temperatures.[26] On the other hand, NMR measurements of the Zn-doped barlowite[27] demonstrate the gapped spin-1/2 spinon excitations.

Recently, Kelly *et al.* have succeeded in a topochemical synthesis of lithium intercalation doped herbertsmithite $[ZnLi_xCu_3(OH)_6Cl_2]$. The electron from the intercalated Li is indeed found doped into the Cu^{2+} kagome spin system, as evidenced by the linear decrease of magnetization as a function of the Li doping concentration. However, contrary to expectations, no metallicity or superconductivity was observed.[28] It is natural to question whether the insulating behavior is due to many-body physics, or chemical reasons. From the many-body physics perspective, insulating behavior in the lightly doped region can be explained using valance bond solid state[29,30] and holon Wigner crystal[31] theory, which have been proposed based on the doped t–J model for QSLs. However, the insulating behavior remains even in the heavily doped region, *e.g.*, $x = 1.8$ with 3e/5 per Cu, which is generally expected to be metallic, as reported in variational Monte Carlo simulations.[29] On the other hand, chemical interactions in the Li-doped herbertsmithite have not been investigated yet, and are known to have a critical influence on the ionic system and may provide an explanation for the insulating behavior with different doping concentrations.

[a] *Department of Materials Science and Engineering, University of Utah, Salt Lake City, Utah 84112, USA. E-mail: fliu@eng.utah.edu*
[b] *Institute for Quantum Science and Engineering, and Department of Physics, Southern University of Science and Technology, Shenzhen 518055, China. E-mail: meijw@sustc.edu.cn*

† Electronic supplementary information (ESI) available. See DOI: 10.1039/c8cp03219j

In this paper, using a first-principles calculation method, we studied the Li intercalation doping effects of the two kagome spin liquid compounds. In the Li-doped herbertsmithite, it was speculated that Li is located in the Cl–$(OH)_3$ tetrahedron hole (T-site).[28] Based on this structure, singlet trapping and electron localization were proposed to explain the insulating behavior. However, we found that Li prefers to sit at the Cl–$(OH)_3$–Cl pentahedron site (square pyramid, P-site), having a total energy of around 0.8 eV per unit cell (u.c.) lower than that of the T-site. Consistent with experiments, we found that the total magnetization decreases linearly with increasing Li doping concentration, which is caused by electron transfer from the intercalated Li to the nearby Cu ions. From projected density of states (PDOS) and crystal orbital Hamilton population (COHP) analysis, we found that Li forms bonding and antibonding states with the neighboring $(OH)^-$ and Cl^- ions. This lowers the neighboring chemical potential, and traps the doped electron in the vicinity of the doped Li, explaining the insulating behavior observed experimentally.[28] Though the newly synthesized compound, Zn-doped barlowite, has a different structure, we found that the doped Li still prefers to locate in the same location and forms chemical bonds with nearby $(OH)^-$ and halogen ions. With the same analysis as the Li-doped herbertsmithite, we expect the same insulating feature will be observed for the Zn-doped barlowite.

2 Calculation methods

Our first-principles calculations were carried out within the framework of the Perdew–Burke–Ernzerhof generalized gradient approximation, as embedded in the Vienna *ab initio* simulation package code.[32] All the calculations were performed with a plane-wave cutoff energy of 500 eV. For structural relaxation, we adopted the experimental lattice constants for both herbertsmithite and Zn-doped barlowite. The geometric optimizations were performed without any constraint until the force on each atom was less than 0.01 eV $Å^{-1}$ and the change of total energy was smaller than 10^{-4} eV per unit cell. The Brillouin zone *k*-point sampling was set with a spacing of $0.03 \times 2\pi$ $Å^{-1}$, which corresponds to a $6 \times 6 \times 4$ and $3 \times 3 \times 4$ *k*-point mesh for the unit-cell, and a $2 \times 2 \times 1$ supercell calculation, respectively. To better describe the localized 3d electrons of Cu, an additional on-site Hubbard *U* term was added in to the calculation of magnetic properties, with different *U* (*J* = 0.9 eV) values (3, 4, 5, 6 eV) tested.[33] Within such a range of *U* values, the change of *U* values only affects the gap size between upper and lower Hubbard bands, which has negligible effect on the Li doping. Therefore, we used the results with a representative *U* value of 6 eV to demonstrate the electronic properties before and after the Li doping for both the $ZnCu_3(OH)_6Cl_2$ and $ZnCu_3(OH)_6FBr$ compounds.

3 Results and discussion

Herbertsmithite has the tetrahedral $R\bar{3}m$ (166) space group with *ABC* stacked Cu^{2+} spin-1/2 kagome planes along the *c* direction, which are separated by non-magnetic ions (Fig. 1). Different locations of the possible Li occupancies have been considered,[28] such as element replacement and interstitial insertion. The optimal site for Li ions in herbertsmithite was proposed to be the Cl–$(OH)_3$ T-site, as highlighted by the green polyhedron in Fig. 1. However, by analyzing the local atomic structure, the space of the Cl–$(OH)_3$ T-site (3.55 $Å^3$) is too narrow for the Li ions, which causes a noticeable lattice distortion after Li insertion. There is more space in the nearby Cl–$(OH)_3$–Cl P-site (8.68 $Å^3$) and the Cl–$(OH)_4$–Cl hexahedron vacancy (H-site, 26.46 $Å^3$), as highlighted by the blue and red polyhedron in Fig. 1, respectively. The pentahedron and the hexahedron share a common Cl–$(OH)_3$ square, while the tetrahedron and the pentahedron share a common Cl–O arris. Fig. 1(c), (d), and (e) show the enlarged T-, P-, and H-sites for Li ions, respectively. The concentration ratio for T-, P-, and H-site is 2 : 6 : 1, indicating that the P-sites potentially have the largest capacity for doped Li ions.

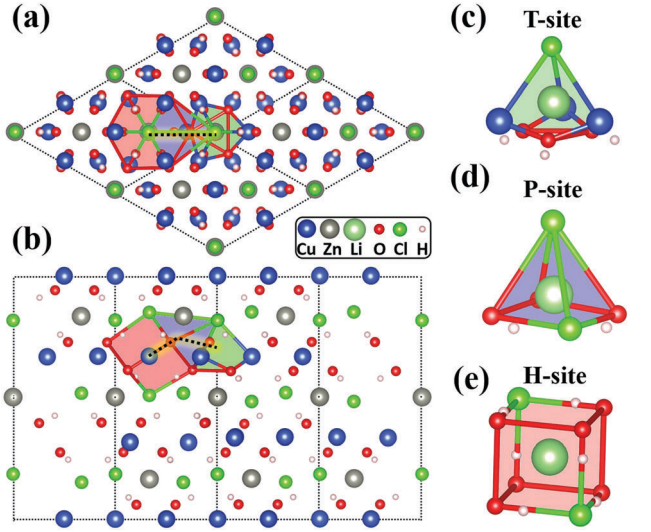

Fig. 1 Li in herbertsmithite. (a) and (b) show the top and side view of vacant space in herbertsmithite with green, blue, and red colors highlighting the tetrahedron (T), pentahedron (P), and hexahedron (H) sites, respectively. The dashed lines indicate the unit cell. (c), (d), and (e) show the possible positions of the Li ion in the T-, P-, and H-sites, respectively.

To determine the most stable position for the doped Li ions in herbertsmithite, we first carried out total-energy calculations with Li ions in these three different locations, *i.e.* the T-, P-, and H-sites. After relaxation, the Li ion in the H-site is relaxed to the off-center position close to hydroxide $(OH)^-$, rather than the assumed cubic center, indicating that Li prefers to bond with $(OH)^-$. We found that the H-site with the largest space is not the most stable position for Li. Instead, the position of Li with the lowest total energy is the P-site, formed by three $(OH)^-$ and two Cl ions, as shown in Fig. 1(d). The structural configuration of Li located in the T-site of a Cl and Cu triangle is found to be metastable [Fig. 1(c)], and has around 0.8 eV per u.c. higher energy than that of the P-site. It is important to mention that due to the small space of the T-site, neighboring Cu and O atoms are greatly distorted after Li insertion, while atomic positions are nearly unchanged for the Li-doping in the

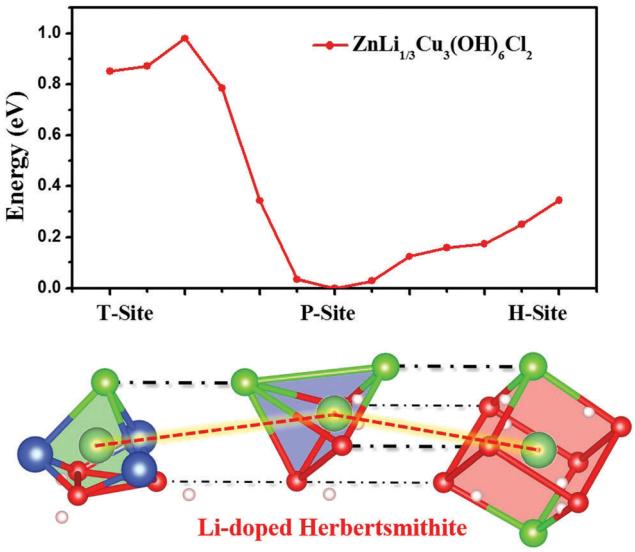

Fig. 2 The nudged elastic band calculation for Li in herbertsmithite. The P-site is found to be the most stable position for Li. The highlighted red dashed lines indicate the path for the calculation.

P- and H-site because of their larger space. To confirm the most stable position of Li in herbertsmithite, we then performed a nudged elastic band (NEB) calculation[34] following the pathway from the T- to P- to H-site, as shown by the highlighted black dashed line in Fig. 1(a) and (b). The results are summarized in Fig. 2, showing that the P-site is indeed the most stable position for Li with a total energy around 0.8 and 0.4 eV per u.c. lower than that of the T- and H-site, respectively. We have further tested 2 × 2 × 1 supercell calculations, which yield the same conclusion that the P-site is the most stable position for Li.

As described by the magnetic susceptibility measurements,[28] the magnetic moment of the Li-doped herbertsmithite decreases linearly with increasing Li doping concentration. Therefore, the electrons of Li are indeed doped into the Cu^{2+} kagome planes. To demonstrate this behavior, we calculated magnetic properties of the Li-doped herbertsmithite and plotted the PDOS of Cu before and after doping, using the most stable structural configuration of Li [Fig. 3(a)]. As shown in Fig. 3(b), before the doping, the PDOS of Cu shows a gapped feature with the upper and lower Hubbard bands located above and below the Fermi level, respectively.

After doping, the PDOS of the Cu ions away from the doped Li [Cu in the red square in Fig. 3(a)] shows a similar gapped feature. The position of the Fermi level relative to the Cu DOS is moderately changed due to the doping effect. However, for the Cu close to the doped Li [the blue square in Fig. 3(a)], the Fermi level is located in the gap of the previous upper Hubbard band of the PDOS [Fig. 3(b)]. This indicates that the Cu ions gain electrons from Li, which results in the decrease of the total magnetic moment. More importantly, the whole system remains gapped, which is consistent with the experiments. It is important to note that near the doped Li ion, there are actually two nearly equidistant Cu ions that share one doped electron. This explains the partial filling rather than the full filling of the d orbitals of

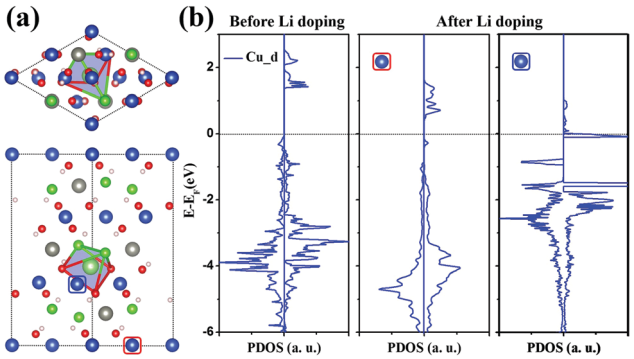

Fig. 3 Li-Doped herbertsmithite. (a) shows the top and side view of the most stable structure configuration for Li in herbertsmithite. The Cu ions in the red and blue squares represent Cu ions that are unaffected and affected by the doped Li, respectively. (b) shows the PDOS of Cu ions before and after the Li doping.

these Cu ions [Fig. 3(b)]. Therefore, the oxidation state of the Cu is actually between Cu^{+} and Cu^{2+}, which is further confirmed by a reduced, rather than vanished, magnetic moment of these Cu ions after Li doping.

Furthermore, we studied the change of the total magnetic moment as a function of Li doping concentration by changing the number of Li ions in the 2 × 2 × 1 supercell. We have calculated four different doping concentrations, *i.e.*, x = 1/12, 1/6, 1/3, and 1 for $ZnLi_xCu_3(OH)_6Cl_2$. All of the Li ions are located in the most stable P-site. Using a ferromagnetic spin configuration to simulate the saturation magnetization, we observed the same linear decrease of magnetic moment as a function of Li doping concentration (Fig. 4), as reported by experiments.[28]

The next mysterious question to be answered is how the doped electrons are trapped in the Cu kagome plane, which leads to the insulating feature observed experimentally. Based on the assumption that Li locates at the T-site,[28] several possible trapping mechanisms considering the strong correlation have been proposed, such as the singlet model and a localized Cu triangle model. However, the optimized position for Li is actually

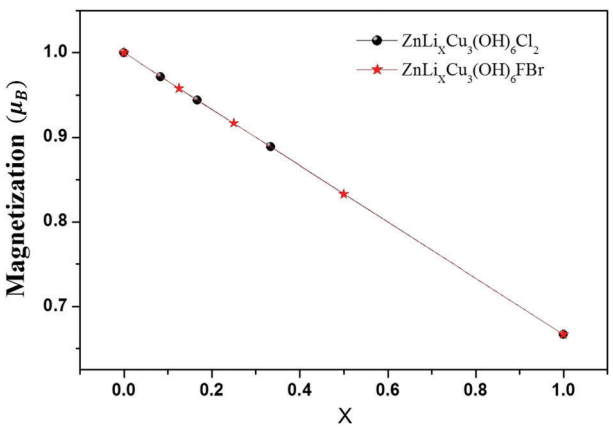

Fig. 4 Change of average magnetic moment on each Cu as a function of Li doping concentration for $ZnLi_xCu_3(OH)_6Cl_2$ (black sphere) and $ZnLi_xCu_3(OH)_6FBr$ (red star).

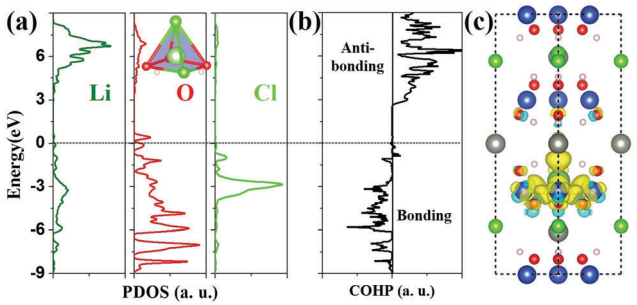

Fig. 5 Chemical bonding in the Li-doped herbertsmithite. (a) Atomic-resolved PDOS. The inset shows the local environment of the Li in the P-site. (b) A COHP curve of the averaged Li–O and Li–Cl bonds. (c) The charge variance distribution with an isosurface level of 0.02.

the P-site and previous theories can only explain the insulating behavior of the lightly doped QSL.[29–31] Therefore, a new mechanism for electron trapping is necessary. It is known that the electronic and magnetic properties of ionic systems can be dramatically affected by the doped ions, such as through chemical bonding between dopant and host ions. If Li bonds with Cl/OH^- forming a LiCl/Li(OH) pair, electrons can be trapped, which leads to the insulating behavior. To test this idea, we further studied the detailed electronic properties of Li and its nearby OH^- and Cl^- ions using the most stable structure.

As shown in Fig. 5(a), we plotted the atomic-resolved PDOS of Li and nearby Cl and O that form a pentagon cage to study their chemical reactions. From the PDOS of Li, it is clear that most of the DOS is located above the Fermi level (5–8 eV), confirming the electron transfer from Li to the nearby Cu ions. There is a little of the DOS below the Fermi level with a relatively large broadening (−8 to 0 eV), showing features of strong hybridization. Importantly, comparing the PDOS of O and Cl to that of Li, we find that their PDOS are located in the exactly same energy range, suggesting possible bonding and anti-bonding features. Different to the wide broadening of O 2p orbitals, the Cl 2p orbitals are more localized. Additionally, the bonding nature of Li–O and Li–Cl were studied using the COHP analysis,[35] as shown in Fig. 5(b). From the averaged COHP curve, the bonding and anti-bonding features are prominent for states below and above the Fermi level, respectively. These chemical reactions lead to a lower chemical potential in the vicinity of the doped Li that traps the electrons on the nearby Cu ions, yielding the insulating feature.

To further support our theory, we plotted the charge variance distribution caused by the doped Li with an isosurface level of 0.02. As shown in Fig. 5(c), the electrons are mainly localized between Li and Cl^-/OH^-, indicating the covalent nature of the Li–Cl/Li–OH bond. This also confirms the electron localization caused by chemical bonding around the Li ion. We additionally examined the size effect using a larger $2 \times 2 \times 1$ supercell, and found similar features of electron localization. It is important to mention that in previous theories,[29–31] the electron doped kagome spin liquids show distinct behaviors under different doping concentrations, *i.e.* insulating and metallic states under lightly and heavily doped conditions, respectively. On the contrary, the chemical reasons described here affect the system consistently in a wide range of Li doping concentrations (0–2e per Cu^{2+}) before structural deformation. This is because the P-sites have a large capacity for holding Li ions with a relatively small structure distortion. Therefore, we believe this could explain why the system was found to remain insulating experimentally under different Li doping concentrations.

Very recently, Zn-doped barlowite has been successfully synthesized, and a gapped quantum spin liquid ground state was revealed.[27] Distinguished from the herbertsmithite with *ABC*-stacked kagome planes, the Zn-doped barlowite has *AA*-stacked Cu^{2+} kagome planes along the *c* direction with the hexagonal $P6_3/mmc$ (193) space group. Nevertheless, we found that the kagome planes formed by Cu and O are identical in these two materials, with very similar local environments. As can be seen from Fig. 6, for both materials, the halogen atoms sit on top of the Cu hexagon center, and the space above the Cu triangle center is occupied by alternating Zn and halogen atoms. Moreover, the T- (3.68 $Å^3$), P- (7.56 $Å^3$), and H-sites (20.79 $Å^3$) in the Zn-doped barlowite are next to each other with a site-ratio of 2 : 6 : 1 [Fig. 7(a)], which are the same as that of the herbertsmithite. Differently, the halogen atom Cl in the herbertsmithite is replaced by Br and F ions in the Zn-doped barlowite, as shown in Fig. 6. Based on total energy calculations for Li in different vacancies of the Zn-doped barlowite, we found that the P-site is also the most stable location for the Li ions, having around 0.9 and 0.5 eV per u.c. lower energy than that of the T- and H-site, respectively. The NEB calculations results are summarized in Fig. 7(b), further confirming the most stable site of the P-site and the metastable state of the T-site for Li in the Zn-doped barlowite.

We then calculated the magnetic properties of the Zn-doped barlowite with different Li doping concentrations. The magnetic behavior of the Zn-doped barlowite upon Li doping is the same as that of the herbertsmithite, in which a linear decrease of magnetization is observed with the increase of Li doping concentration (Fig. 4). This is caused by the charge transfer from the Li ions to nearby Cu ions. Similarly, through PDOS and

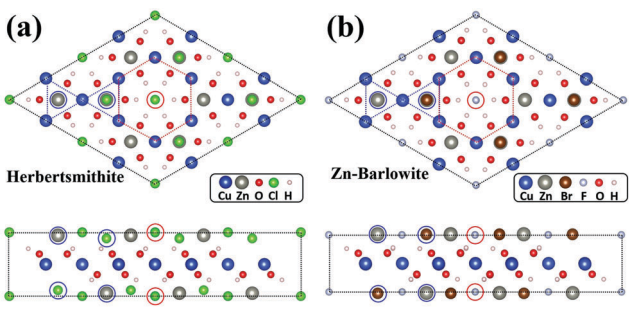

Fig. 6 Local environments of the Cu kagome plane in herbertsmithite and Zn-doped barlowite. (a) and (b) show the top and side view of the Cu kagome plane in herbertsmithite and Zn-doped barlowite, respectively. For herbertsmithite/Zn-doped barlowite, halogen atoms Cl/F (red circle) sit on top of the Cu hexagon center (red hexagon) and the space above and below the Cu triangle (blue triangle) is occupied by Zn and Cl/Br (blue circles) alternatively.

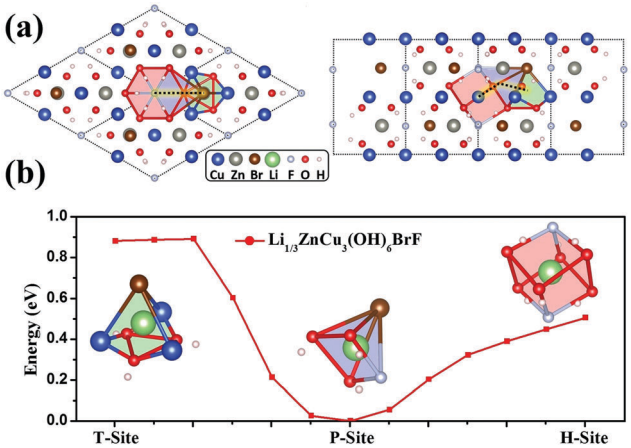

Fig. 7 Li positions in Zn-doped barlowite. (a) shows the top and side view of vacant spaces in the Zn-doped barlowite with green, blue, and red colors highlighting the T-, P-, and H-site, respectively. (b) The NEB calculation results for possible positions of Li ion along the path from T-site to P-site to H-site.

COHP analysis (see ESI†), we found that Li forms chemical bonds with the neighboring OH^-, Br^-, and F^- ions. These bonds lower the chemical potential of the nearby region, leading to electron localization. Therefore, we expect that for the Zn-doped barlowite, Li doping will also yield the same insulating behavior as that of the Li-doped herbertsmithite, even in the heavily doped region. For the same reason, other interstitial doping methods with different elements would not succeed either. In order to realize exotic metallic states, *i.e.* doping electrons into the Cu kagome plane without any restrictions, the doping method must avoid chemical changes close to the Cu kagome plane, or involve chemical changes that have negligible effect to the Cu ions. To meet these requirements, substitution of the inter-kagome plane metal ion, zinc,[36] using other metal ions with a similar radius but different electronic configurations, *e.g.*, Sc, Zr, and Nb, may be feasible (see ESI†).

4 Conclusions

In conclusion, we have carried out a comprehensive study of the Li intercalation doping effect of two promising compounds for 2D realization of kagome spin liquids, *i.e.* herbertsmithite and Zn-doped barlowite. Though with different layer stacking sequences for the Cu kagome planes, the interstitial vacancies are surprisingly alike for these two compounds, which leads to very similar behaviors upon Li doping. Instead of the previously speculated T-site, the P-site was found to be the most stable position for the doped Li ions. It has around 0.8 and 0.9 eV per u.c. lower energy than that of Li in the T-site for herbertsmithite and the Zn-doped barlowite, respectively. We demonstrated the charge transfer from the doped Li to its adjacent Cu ions, which leads to the linear decrease of the saturation magnetization as a function of Li doping concentration. Due to the chemical bonds formed between Li and nearby OH^-, Cl^-, and F^- ions, the chemical potential in the vicinity of Li is substantially lowered. This affects the nearby Cu ions and causes electron localization, giving rise to the insulating behavior even under heavily doped regions. Like many other normal ionic compounds, whose electronic and magnetic properties are greatly affected by chemical reactions upon ionic doping, we have demonstrated that chemical reactions also play a critical role in determining the behaviors of this family of kagome spin liquid compounds with strong correlations. Finally, we propose that to realize exotic metallic states, suitable element substitution (*e.g.*, substitution of Zn with Sc) that avoid chemical changes near the Cu kagome plane may be promising. Our study paves the way for studies of electron doping kagome spin liquids.

Conflicts of interest

There are no conflicts of interest to declare.

Acknowledgements

This project is supported by the U.S. DOE-BES (Grant No. DE-FG02-04ER46148). W. Jiang is additionally supported by the National Science Foundation-Material Research Science & Engineering Center (NSF-MRSEC Grant No. DMR-1121252). We thank the CHPC at the University of Utah and the DOE-NERSC for providing the computing resources.

References

1 P. W. Anderson, *Science*, 1987, **235**, 1196–1198.
2 X. Wen, *Quantum Field Theory of Many-Body Systems: From the Origin of Sound to an Origin of Light and Electrons*, OUP, Oxford, 2004.
3 A. Kitaev and J. Preskill, *Phys. Rev. Lett.*, 2006, **96**, 110404.
4 M. Levin and X.-G. Wen, *Phys. Rev. Lett.*, 2006, **96**, 110405.
5 K.-Y. Yang, T. M. Rice and F.-C. Zhang, *Phys. Rev. B: Condens. Matter Mater. Phys.*, 2006, **73**, 174501.
6 E. G. Moon and S. Sachdev, *Phys. Rev. B: Condens. Matter Mater. Phys.*, 2011, **83**, 224508.
7 J.-W. Mei, S. Kawasaki, G.-Q. Zheng, Z.-Y. Weng and X.-G. Wen, *Phys. Rev. B: Condens. Matter Mater. Phys.*, 2012, **85**, 134519.
8 J.-W. Mei, *Phys. Rev. Lett.*, 2012, **108**, 227207.
9 T. Senthil, S. Sachdev and M. Vojta, *Phys. Rev. Lett.*, 2003, **90**, 216403.
10 T. Senthil, M. Vojta and S. Sachdev, *Phys. Rev. B: Condens. Matter Mater. Phys.*, 2004, **69**, 035111.
11 P. A. Lee, *Science*, 2008, **321**, 1306–1307.
12 L. Balents, *Nature*, 2010, **464**, 199–208.
13 M. R. Norman, *Rev. Mod. Phys.*, 2016, **88**, 041002.
14 S. Depenbrock, I. P. McCulloch and U. Schollwöck, *Phys. Rev. Lett.*, 2012, **109**, 067201.
15 Y. Iqbal, F. Becca, S. Sorella and D. Poilblanc, *Phys. Rev. B: Condens. Matter Mater. Phys.*, 2013, **87**, 060405.
16 S.-S. Gong, W. Zhu, L. Balents and D. N. Sheng, *Phys. Rev. B: Condens. Matter Mater. Phys.*, 2015, **91**, 075112.

17 J.-W. Mei, J.-Y. Chen, H. He and X.-G. Wen, *Phys. Rev. B*, 2017, **95**, 235107.
18 Y.-C. He, M. P. Zaletel, M. Oshikawa and F. Pollmann, *Phys. Rev. X*, 2017, **7**, 031020.
19 S. Jiang, P. Kim, J. H. Han and Y. Ran, arXiv preprint arXiv:1610.02024, 2016.
20 H. J. Liao, Z. Y. Xie, J. Chen, Z. Y. Liu, H. D. Xie, R. Z. Huang, B. Normand and T. Xiang, *Phys. Rev. Lett.*, 2017, **118**, 137202.
21 W. Jiang, Z. Liu, J.-W. Mei, B. Cui and F. Liu, arXiv preprint: 1711.09931, 2017.
22 M. P. Shores, E. A. Nytko, B. M. Bartlett and D. G. Nocera, *J. Am. Chem. Soc.*, 2005, **127**, 13462–13463.
23 J. S. Helton, K. Matan, M. P. Shores, E. A. Nytko, B. M. Bartlett, Y. Yoshida, Y. Takano, A. Suslov, Y. Qiu, J.-H. Chung, D. G. Nocera and Y. S. Lee, *Phys. Rev. Lett.*, 2007, **98**, 107204.
24 P. Mendels, F. Bert, M. A. de Vries, A. Olariu, A. Harrison, F. Duc, J. C. Trombe, J. S. Lord, A. Amato and C. Baines, *Phys. Rev. Lett.*, 2007, **98**, 077204.
25 T.-H. Han, J. S. Helton, S. Chu, D. G. Nocera, J. A. Rodriguez-Rivera, C. Broholm and Y. S. Lee, *Nature*, 2012, **492**, 406–410.
26 M. Fu, T. Imai, T.-H. Han and Y. S. Lee, *Science*, 2015, **350**, 655–658.
27 Z. Feng, Z. Li, X. Meng, W. Yi, Y. Wei, J. Zhang, Y.-C. Wang, W. Jiang, Z. Liu, S. Li, F. Liu, J. Luo, S. Li, G. Qing Zheng, Z. Y. Meng, J.-W. Mei and Y. Shi, *Chin. Phys. Lett.*, 2017, **34**, 077502.
28 Z. A. Kelly, M. J. Gallagher and T. M. McQueen, *Phys. Rev. X*, 2016, **6**, 041007.
29 S. Guertler and H. Monien, *Phys. Rev. B: Condens. Matter Mater. Phys.*, 2011, **84**, 174409.
30 S. Guertler and H. Monien, *Phys. Rev. Lett.*, 2013, **111**, 097204.
31 H.-C. Jiang, T. Devereaux and S. A. Kivelson, *Phys. Rev. Lett.*, 2017, **119**, 067002.
32 G. Kresse and J. Hafner, *Phys. Rev. B: Condens. Matter Mater. Phys.*, 1993, **47**, 558–561.
33 W. Jiang, M. Zhou, Z. Liu, D. Sun, Z. V. Vardeny and F. Liu, *J. Phys.: Condens. Matter*, 2016, **28**, 176004.
34 H.-B. Zhou, N. K. Momanyi, Y.-H. Li, W. Jiang and X.-C. Li, *RSC Adv.*, 2016, **6**, 103622–103631.
35 R. Dronskowski and P. E. Bloechl, *J. Phys. Chem.*, 1993, **97**, 8617–8624.
36 Z. Liu, X. Zou, J.-W. Mei and F. Liu, *Phys. Rev. B: Condens. Matter Mater. Phys.*, 2015, **92**, 220102.

